FUV Emission from AGB Stars: Modeling Accretion Activity associated with a Binary Companion

Alyx Catherine Stevens

NASA Jet Propulsion Laboratory

Major: Astronomy

USRP Fall 2012

Date: 21 December 2012

FUV Emission from AGB Stars: Modeling Accretion Activity associated with a Binary Companion

Alyx Catherine Stevens[1] and Raghvendra Sahai[2]
Jet Propulsion Laboratory, California Institute of Technology, NASA, La Canada Flintridge, CA, 91011

It is widely believed that the late stages of evolution for Asymptotic Giant Branch (AGB) stars are influenced by the presence of binary companions. Unfortunately, there is a lack of direct observational evidence of binarity. However, more recently, strong indirect evidence comes from the discovery of UV emission in a subsample of these objects (fuvAGB stars). AGB stars are comparatively cool objects (≤ 3000 K), thus their fluxes falls off drastically for wavelengths 3000A and shorter. Therefore, ultraviolet observations offer an important, new technique for detecting the binary companions and/or associated accretion activity. We develop new models of UV emission from fuvAGB stars constrained by GALEX photometry and spectroscopy of these objects. We compare the GALEX UV grism spectra of the AGB M7 star EY Hya to predictions using the spectral synthesis code Cloudy, specifically investigating the ultraviolet wavelength range (1344-2831Å). We investigate models composed of contributions from a photoionized "hot spot" due to accretion activity around the companion, and "chromospheric" emission from collisionally ionized plasma, to fit the UV observations.

1. Introduction

It is a common belief that the late stages of stellar evolution are influenced by the presence of a binary companion (e.g., Balick & Frank 2002). This belief is generated in the difficulties single-star models have in explaining the drastic change in morphologies for low to medium-mass Asymptotic Giant Branch (henceforth AGB) stars transitioning into the planetary nebula phase (e.g., Garcia-Segura 1997). Their roughly spherical envelopes transform into a conglomeration of asymmetrical shapes (e.g. Sahai & Trauger 1998). Binarity amongst AGB stars, however, proves tough to observe directly. AGB stars possess a high luminosity of about 10^4 L_{sun}, significantly more luminous then the stellar companion, assumed to be a main-sequence star or white dwarf. Due to a lack of direct observational evidence proving the binarity of these objects, we must find alternate methods to prove that these AGB possess binary companions.

AGB stars are comparatively cool objects of spectral type M6 or later, thus their fluxes falls off drastically for wavelengths 3000 Å and shorter. Therefore, ultraviolet photometry offers an important, new technique for determining the binarity of AGB stars. Using that technique, Sahai et al. (2008) found a sample of AGB stars with strong UV excess (henceforth "fuvAGB" stars). In this study, we look at the UV emission from fuvAGB stars taken from Sahai et al. (2008a), but narrow down on the object EY Hya, in particular. EY Hya is a semi-regular pulsating M7 AGB star at an assumed distance of 600 pc, using the Hipparcos parallax (1.66" ± 1.01"). EY Hya is of particular interest because the observed far ultraviolet

---

[1] USRP Intern, Astrophysics and Space Sciences, Jet Propulsion Laboratory, University of Texas at Austin.
[2] Research Scientist, Astrophysics and Space Sciences, 4800 Oak Grove Dr. M/S 183-900, Jet Propulsion Laboratory.

(FUV) flux is a factor ~10^6 larger than expected for the photospheric emission of the primary, leading to the conclusion that the UV excess in EY Hya is due to either the presence of a hot binary companion or from accretion activity associated with a "hot spot" located on an accretion disk or on the companion's surface.

We model the FUV and NUV data acquired from GALEX using calculations performed with version 08.00 of the astrophysical plasma simulating code Cloudy (Ferland et al. 1998). One fuvAGB star, V Hya, which has the largest FUV flux as well as the highest FUV-to-NUV flux ratio among the target objects of Sahai et al. (2008), was recently observed with the Hubble Space Telescope (HST) Imaging Spectrograph (STIS) and showed the presence of a high-velocity emission-line blob projected to be moving away from V Hya at 220 km/s. In addition to this blob, a hot expanding disk-shaped structure was revealed, though not an accretion disk due to the expansive nature of the latter (Sahai et al. 2003). As a side benefit of our modeling, we use Cloudy to model the optical spectrum of this emission-line blob in V Hya.

Our study is related to the effects of binarity in understanding the death of Sun-like stars. This evolutionary phase is a crucially important part of the life cycle of these stars, because in their death throes, these objects sow the seeds (in the form of dust grains and nucleosynthesis products) for the birth of new stars and solar systems. This work is thus related to the Astronomical Search for Origins & Planetary Systems and the Destiny, Structure & Evolution of the Universe themes in NASA's SMD Science Plan (2007-2016). These themes address, among other topics, the origins of stars, protoplanetary and extra-solar planetary systems, and the origin of life; and the evolution of stars and galaxies, including the Milky Way.

2. Summary of Observations

2.1 GALEX Data

UV spectra of a small sample of fuvAGB stars were acquired with GALEX's grism instrument via a Cycle 5 GI program # GI5-054, entitled "Probing Binary Companions and Accretion Disks in AGB stars" (Sahai et al. 2008b). This sample includes EY Hya, whose prominent UV emission was discovered from examination of the GALEX archive (Sahai et al. 2008). This is the only object with both FUV and NUV grism spectra (the FUV detector stopped functioning before the rest of the sample was observed). The fluxes (or upper limits) of major emission lines in EY Hya's spectrum are given in Table 1.

We selected EY Hya for a detailed study, because, as stated by Deeb & Sahai (2012), "EY Hya's spectrum contains a significant FUV flux (relative to the strongest NUV features) with the flux of the strongest features totaling to about 1.10×10^{-13} ergs s^{-1} cm^{-2} Å. It is possible that there exists a combination of a UV continuum with emission lines extending beyond. EY Hya contains a large number what appear to be FUV features that are similar to those found in the study of Mira B (Reimers & Castella 1985) as well as in the study of accreting pre-main sequence stars (Ingleby et al. 2011) and of CI Cygni (Kenyon et al. 1991)." The broadband photometry of fuvAGB objects with a grism spectra is summarized in Table 2.

TABLE 1
LINE FLUXES FOR EY HYA

Flux ($erg\ s^{-1}\ cm^{-2}$)				
Mg II 2800 Å	**C II 2336 Å**	**Fe II 2400 Å**	**Si III 1888 Å**	**Al II 2670 Å**
7.1×10^{-14}	1.3×10^{-14}	$< 1.3 \times 10^{-15}$	$< 1.0 \times 10^{-14}$	$< 1.51 \times 10^{-15}$

Upper limits are 1 sigma

TABLE 2
BROADBAND DATA FOR FUVAGB OBJECTS

Object	Epoch Identifier[a]	Distance (Parsecs)	FUV_{flux} erg/s/cm^2	NUV_{flux} erg/s/cm^2	Data Source (if applicable)
EY Hya[b]	2006-02-20	600	6.86×10^{-28}	8.79×10^{-28}	AIS
	2007-02-19		9.50×10^{-28}	1.336×10^{-27}	MIS
V Hya	3421.86	690	1.2×10^{-27}	1.1×10^{-27}	Sahai et al. (2008a)
	3778.54		1.5×10^{-27}	1.3×10^{-27}	Sahai et al. (2008a)
V Eri	3678.2	440	6×10^{-28}	1.4×10^{-27}	Sahai et al. (2008a)
AA Cam	3377.48	780	1.4×10^{-28}	2.2×10^{-27}	Sahai et al. (2008a)
EP Aqr	2006-08-20	110	6.54×10^{-29}	1.98×10^{-27}	MIS
	2006-09-29		1.05×10^{-28}	2.69×10^{-27}	MIS
R UMa	3742.14	410	1.1×10^{-28}	1.2×10^{-27}	Sahai et al. (2008a)
TW Hor	3349.3	320	2.6×10^{-28}	5.3×10^{-27}	Sahai et al. (2008a)
	3351.2		3.2×10^{-28}	5.5×10^{-27}	Sahai et al. (2008a)
	3671.8		3.4×10^{-28}	7.8×10^{-27}	Sahai et al. (2008a)
	3706.6		2.3×10^{-28}	2.6×10^{-27}	Sahai et al. (2008a)
	3706.7		3.3×10^{-28}	2.7×10^{-27}	Sahai et al. (2008a)
	4018.8		3.4×10^{-28}	9.9×10^{-27}	Sahai et al. (2008a)
TZ Hor	2006-08-29	230	6.51×10^{-28}	1.04×10^{-26}	AIS
VY UMa	3742.5	380	6.1×10^{-29}	5.3×10^{-27}	Sahai et al. (2008a)
W Peg	2006-10-02	290	1.31×10^{-28}	2.01×10^{-27}	AIS

[a] Either in calendar date or Julian Day format, JD -2,450,000 if latter.
[b] EY Hya's grism epoch is 2009-02-07

2.2 Optical Spectrum of V Hya

In addition to the broadband photometry data of the fuvAGB objects, we also have optical spectra for the object V Hya (Lloyd Evans, private communication, 2011). Prominent optical emission lines in for V Hya were measured and are listed in Table 3. These were measured using the "splot" tool in IRAF to plot and analyze spectra, using a Gaussian fit.

TABLE 3
OPTICAL SPECTRUM DATA FOR V HYA

		Flux ($erg\ s^{-1}\ cm^{-2}$)						
Epoch	**Epoch Identifier**	**Ca II 3931 Å**	**Ca II 3934 Å**	**S II 4066 Å**	**S II 4074 Å**	**Sr II 4213 Å**	**Fe II 4247 Å**	**Fe II 4285 Å**
2001-02-05	7444	3.77×10^{-15}	2.88×10^{-15}	4.28×10^{-14}	1.76×10^{-14}	3.82×10^{-15}	1.26×10^{-14}	1.15×10^{-14}
2001-03-06	7630	3.62×10^{-15}	5.51×10^{-15}	2.89×10^{-14}	1.02×10^{-14}	2.66×10^{-15}	1.15×10^{-14}	1.07×10^{-14}
2001-11-10	8105	8.52×10^{-15}	3.41×10^{-14}	5.74×10^{-14}	4.05×10^{-14}	1.61×10^{-14}	1.99×10^{-14}	2.07×10^{-14}
2001-11-10	8134	9.53×10^{-15}	6.45×10^{-14}	5.32×10^{-14}	3.12×10^{-14}	1.55×10^{-14}	1.62×10^{-14}	1.32×10^{-14}

3. Modeling

3.1 Two-Component Model

When modeling EY Hya, we were motivated to create a two-component model; a photoionized hot spot due to accretion activity, and a collisionally ionized chromosphere. A two-component model was needed because using either component independently did not correctly model EY Hya. The photoionized accretion activity hot spot component, while producing the correct continuum did not produce any observed emission lines besides CII] 2332 Å. The collisionally ionized chromosphere component produced the observed emission lines, but did not produce our observed continuum. Thus, a combination model of the two components is required.

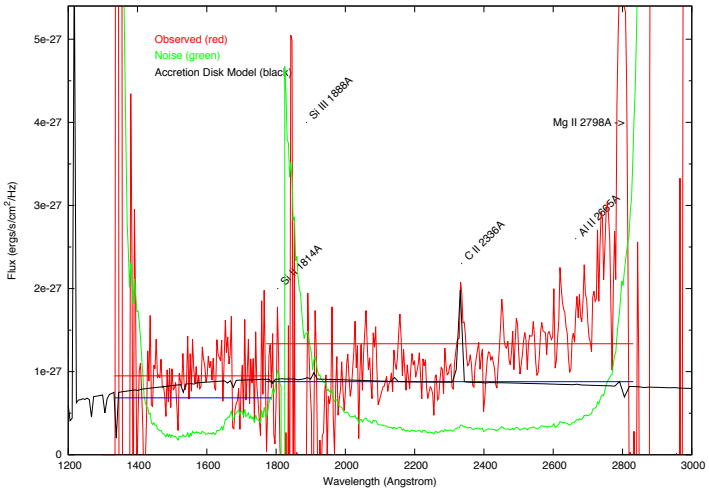

Figure 1. Accretion Activity Hot Spot Component for EY Hya. *Modeled with an accretion temperature of 27,000 K, luminosity of 33 (log erg/s), hydrogen density of 5.5 (log cm^{-3}), an inner radius of 10^{13} cm, outer radius of 10^{15} cm, and a scale factor, F_{accr}, of 0.11. The model was created to fit the EY Hya FUV/NUV fluxes taken from two separate surveys: AIS 2006-02-20 and MIS 2007-02-19. Observed (red), noise (green), accretion activity hot spot component (black.).*

3.1.1 Accretion Activity Hot Spot, Model Component no. 1

We create a two-component model for EY Hya; our first component calculates the effects of photoionization and simulates the effect of accretion activity onto a hot spot. Here we vary the major and physical parameters (to be discussed below) to reproduce the continuum slope over the FUV and NUV λ bands and the CII] 2332 Å line, (Fig. 1). The wavelength region, $\lambda \geq 2400$ Å where the continuum starts rising, (due to the "tail" of the photospheric emission from the cool but very luminous AGB star) is ignored in fitting the continuum slope. Because our accretion activity hot spot model doesn't produce any of the observed emission lines besides CII] 2332 Å, we were then motivated to include the second component, to be discussed in 3.1.2.

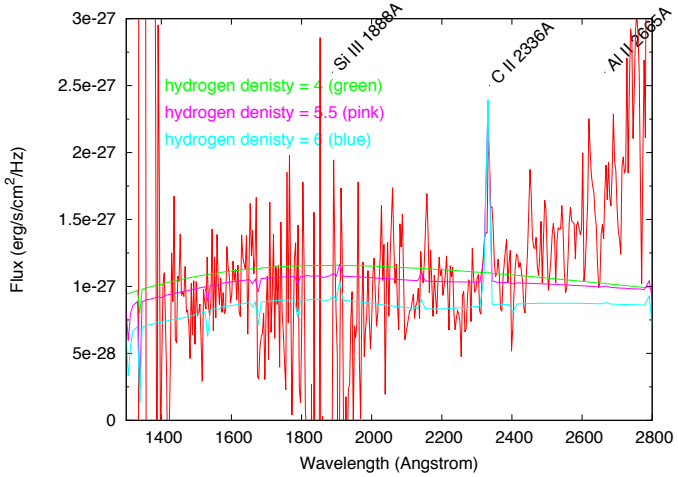

Figure 2. Accretion Activity Hot Spot Component with varying Hydrogen Densities. *Modeled with a temperature of 27,000 K, an inner radius of 10^{13} cm and an outer radius of 10^{15} cm. Observed (red), h.den. = 4 (green), h.den. = 5.5 (pink), h.den. = 6 (blue). Hydrogen Densities in units log cm^{-3}.*

For our accretion activity hot-spot component, we vary two important input parameters: the temperature of the blackbody, T_{bb}, and the hydrogen density. For this component we use the command

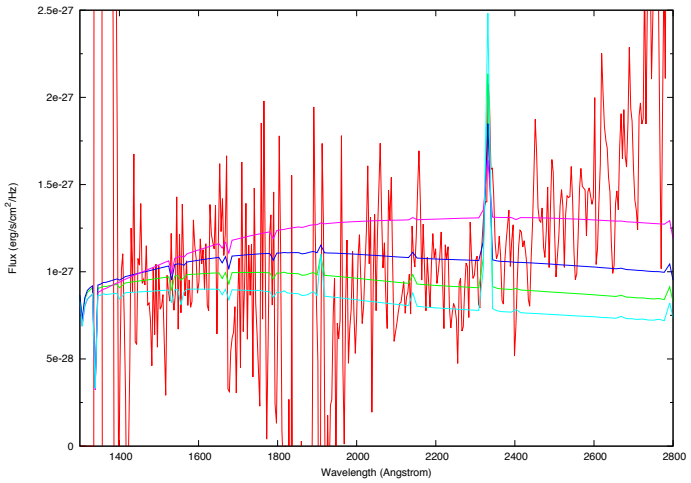

Figure 3. Accretion Activity Hot Spot Component with varying T_{bb}. *Modeled with a hydrogen density of $10^{5.5}$ cm^{-3}, an inner radius of 10^{13} cm and an outer radius of 10^{15} cm. Observed (red), T=33,000 K (light blue), T=30,000 K (green), T=27,000 K (blue), T=23,000 K (pink).*

"abundances planetary nebula" which specifies a pre-conceived mixture of gas and dust that is appropriate as resulting from nuclear processing and dust formed during the AGB evolutionary phase. (For a detailed description of what the output code produces, refer to the Appendix, A.1.)

Varying these parameters allows us to get an accurate prediction of EY Hya's continuum spectrum. Changing the hydrogen density changes the strength of the few lines present in the model spectrum (Fig. 2). Changing the temperature of the blackbody changes the shape of the continuum (Fig. 3). Changing the luminosity simply scales the continuum up or down. Hence the arbitrary scale factor, F_{acc}, applied to the model spectrum to fit the observed continuum intensity, is equivalent to varying the luminosity (Fig. 1).

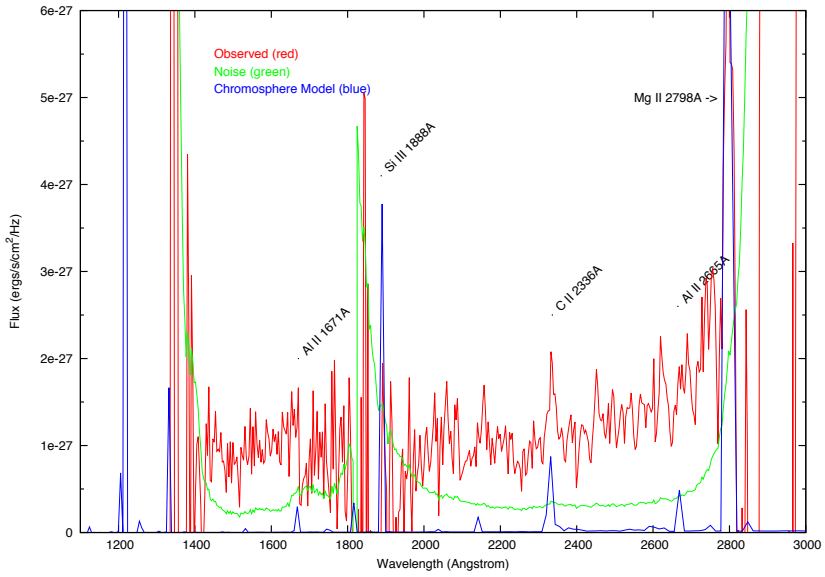

Figure 4. Chromospheric Component for EY Hya. *Modeled with a coronal temperature of 19,000 K, hydrogen density of 10.5 (log cm^{-3}), an inner radius of 10^{11} cm, an outer radius of $10^{11.04}$ cm, and a scale factor, F_{chr} , of 0.75. Observed (red), noise (green), chromosphere component (blue).*

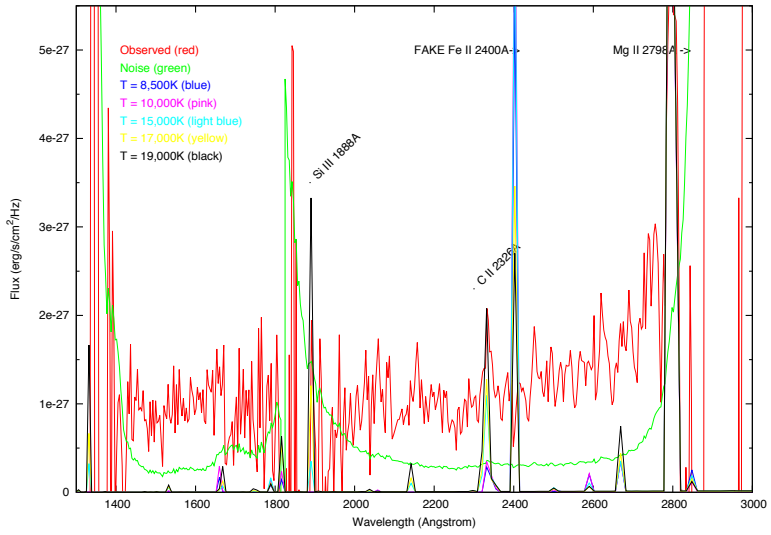

Figure 6. Chromospheric Model with varying Temperature. *Modeled with hydrogen density of 10 (log cm^{-3}), inner radius 10^{11} cm and an outer radius of $10^{11.04}$ cm. Observed (red), noise (green), T=8,500 K (blue), T=10,000 K (pink), T=15,000 K (light blue), T=17,000 K (yellow), T=19,000 K (black). The command "atom FeII 371" was not used in the input, and thus a fake Fe II line at 2400 A is produced (section 3.1.2.3).*

3.1.2 Chromospheric Emission, Model Component no. 2

A plausible model to create emission lines is that of a hot, collisionally ionized region, namely a chromosphere that comes from around a companion or the AGB star itself (Skinner et al. 1997). Therefore, the second component simulates the effects of collisional excitation in a hot chromosphere. For our chromosphere model, we vary two important factors the temperature of the chromosphere, T_{chr},[2] and the hydrogen density. We also specify the "geometry" of the gas (see A.2). We have assumed a solar composition for abundances. An arbitrary scale factor, F_{chr}, is applied to the model spectrum, and adjusted for each model in order to fit the observed Mg II line intensity. Variations in F_{chr} are equivalent to changes in parameters that simply scale the spectrum up or down. (For further details on input parameters for the chromosphere component, refer to the Appendix, A.2.)

Varying these parameters obviously generates different results than what we saw in the accretion disk. Varying the hydrogen density is particularly important in the chromosphere model. Lowering the hydrogen density increases the strength of lines at longer wavelength with no effect on lines at shorter wavelengths, and vice versa (Fig. 5). Increasing the temperature produces an abundance of additional lines, as well as increasing the strengths of lines at shorter wavelengths (Fig. 6). Additional input parameters include the inner radius of the cloud, r_{in}, and the outer radius of the cloud, r_{out}. Changing the inner radius only changes the scale of the flux up or down in relation to the object's spectrum, the same effect we saw previously in the accretion disk model when changing the luminosity. Changing the outer radius changes the line strengths in relation to each other (Fig. 4).

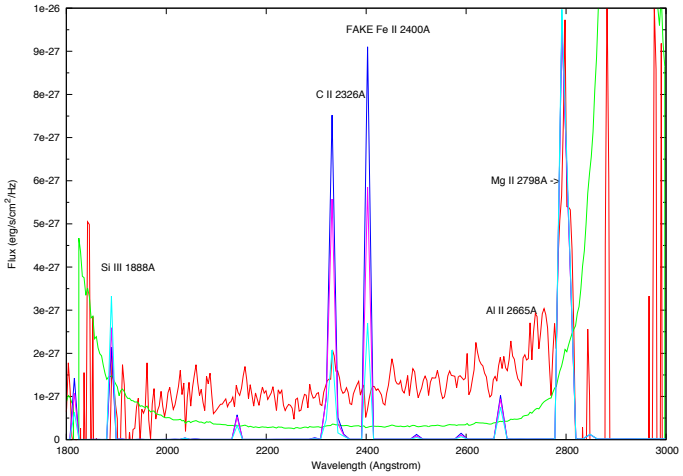

Figure 5. Chromospheric Component with varying Hydrogen Density. *Modeled with T_{chr}=19,000 K, $r_{in}=10^{11}$ cm, $r_{out}=10^{11.04}$ cm. Notice this model was not run using the "atom FeII 371" command (section 3.1.2.3), therefore contains a fake Fe II line at 2400 A. Observed (red), noise (green), h.den.=10 (light blue), h.den.=9 (pink), and h.den.=8 (blue). Hydrogen Densities in units log cm^{-3}.*

[2] Refer to Appendix A.3 for explanation of chromosphere temperature

3.1.2.1 Emergent Line Intensities

We explore the dependence of the FUV/NUV line fluxes on various physical parameters, e.g. chromosphere temperature and hydrogen density, utilizing the emergent line intensities listed in the output from Cloudy (for more information on the Cloudy output files, see Appendix A.1). Table 4 shows how the line flux for the prominent emission lines in the UV (Mg II at 2798 Å, CII] at 2326 Å, Si III] at 1888 Å, and Al II at 1671 Å) vary as a function of hydrogen density. Table 5 shows how these same lines vary as a function of chromospheric temperature

TABLE 4

LINE FLUX DEPENDENCE ON HYDROGEN DENSITY IN CHROMOSPHERIC MODEL

				Flux ($erg\ s^{-1}\ cm^{-2}$)				
T_{chr} (K)	**r_{in}** (cm)	**r_{out}** (cm)	**Hydrogen Density** (cm^{-3})	**Mg II 2798 Å**	**C II] 2326 Å**	**Si III] 1888 Å**	**Al II 1671 Å**	**F_{chr}**
$1.9x10^4$	10^{11}	$10^{11.04}$	10^8	$8.96x10^{-19}$	$5.64x10^{-19}$	$7.85x10^{-22}$	$6.56x10^{-20}$	$8.8x10^4$
			10^9	$9.77x10^{-17}$	$4.75x10^{-17}$	$1.08x10^{-19}$	$6.64x10^{-18}$	$8.0x10^2$
			10^{10}	$1.08x10^{-14}$	$1.86x10^{-15}$	$5.29x10^{-18}$	$5.57x10^{-16}$	7.5
			10^{11}	$8.89x10^{-13}$	$2.58x10^{-14}$	$2.59x10^{-16}$	$1.92x10^{-14}$	(a)
			10^{12}	$1.10x10^{-11}$	$2.43x10^{-13}$	$3.11x10^{-14}$	$2.07x10^{-13}$	(a)

(a) F_{chr} value in model database, not provided here

TABLE 5

LINE FLUX DEPENDENCE ON CORONAL TEMPERATURE IN CHROMOSPHERIC MODEL

				Flux ($erg\ s^{-1}\ cm^{-2}$)				
Hydrogen Density (cm^{-3})	**r_{in}** (cm)	**r_{out}** (cm)	**T_{chr}** (K)	**Mg II 2798 Å**	**C II] 2326 Å**	**Si III] 1888 Å**	**Al II 1671 Å**	**F_{chr}**
10^{10}	10^{11}	$10^{11.04}$	$1.1x10^3$	$3.63x10^{-17}$	$3.86x10^{-19}$	$4.77x10^{-22}$	$9.31x10^{-19}$	(a)
			$1.4x10^4$	$8.85x10^{-15}$	$5.72x10^{-16}$	$1.51x10^{-16}$	$2.07x10^{-16}$	(a)
			$1.9x10^4$	$1.08x10^{-14}$	$1.86x10^{-15}$	$3.56x10^{-15}$	$5.57x10^{-16}$	7.5
			$2.4x10^4$	$2.95x10^{-15}$	$3.34x10^{-15}$	$9.12x10^{-15}$	$8.47x10^{-16}$	(a)
			$2.9x10^4$	$9.38x10^{-16}$	$4.22x10^{-15}$	$1.33x10^{-14}$	$9.49x10^{-16}$	(a)

(a) F_{chr} value in model database, not provided here

Figures 7, 8, and 9 show the line flux ratios for CII]/MgII, AlII/MgII, and SiIII/MgII, as a function of temperature, hydrogen density, and volume, respectively. Comparison of the line flux ratios from Cloudy are made to measurements of the line flux ratios from EY Hya. From these line flux ratios, we see that the best parameters to model EY Hya is T_{chr} ~19,000 K (Fig. 7) and a hydrogen density ~10^{10} cm^{-3} (Fig. 8). We find that we cannot constrain the volume because the line flux ratios are not significantly sensitive to changes in volume (Fig. 9). The outer radius was the input parameter varied to change the volume.

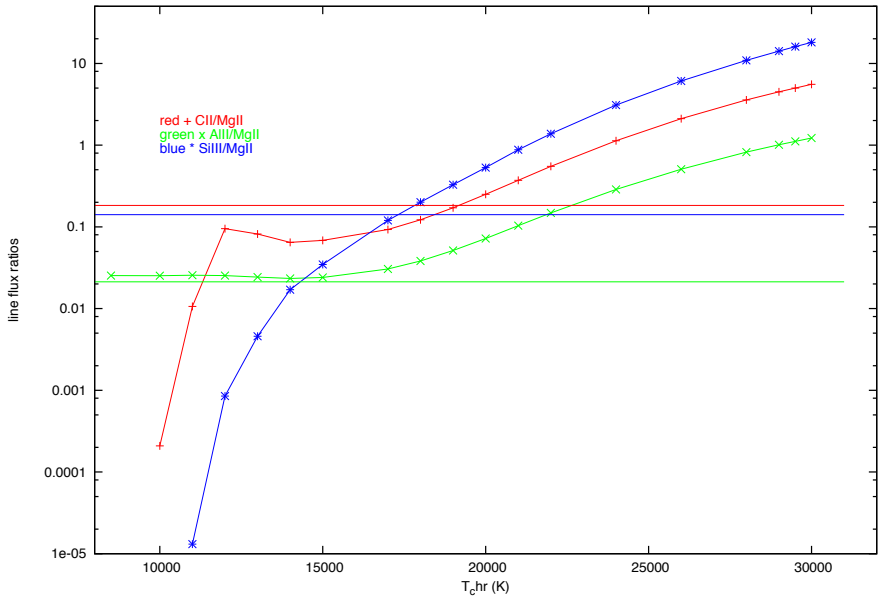

Figure 7. Line Flux Ratios from Chromospheric Model as a function of T_{chr}. *Ratios include CII]/Mg II (red), Al II/MgII (green), SiIII/MgII (blue). Lines with points show Cloudy predictions, while flat lines are observed line ratios from EY Hya. Hydrogen density =10^{10} cm^{-3}, r_{in} =10^{10} cm, r_{out} =$10^{11.04}$ cm were kept fixed for all models.*

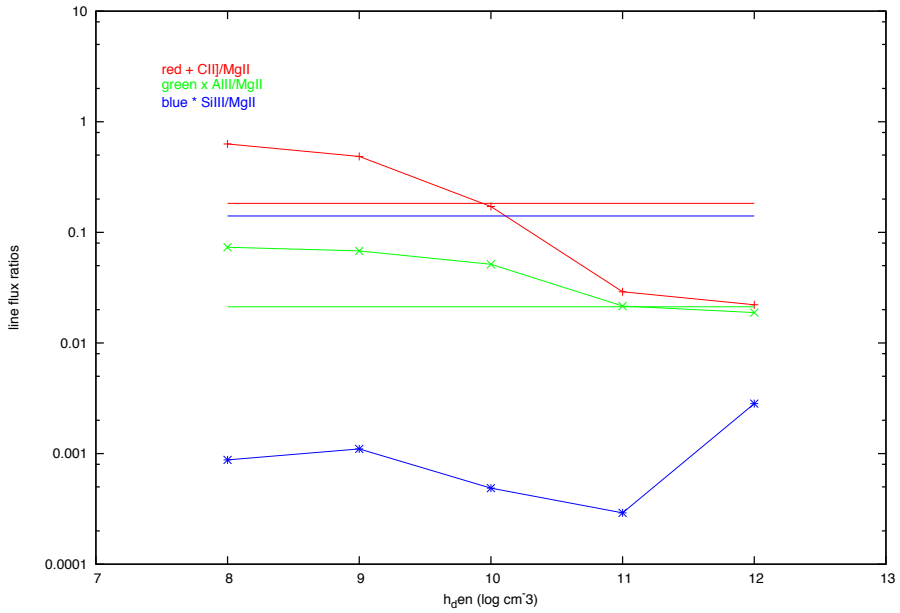

Figure 8. Line Flux Ratios of Chromospheric Model with changing hydrogen density. *Ratios include CII]/Mg II (red), Al II/MgII (green), SiIII/MgII (blue). Lines with points show Cloudy predictions, while flat lines are observed line ratios from EY Hya. T_{chr} =1.9x10^{4} K, r_{in} =10^{10} cm, r_{out} =$10^{11.04}$ cm were kept fixed for all models.*

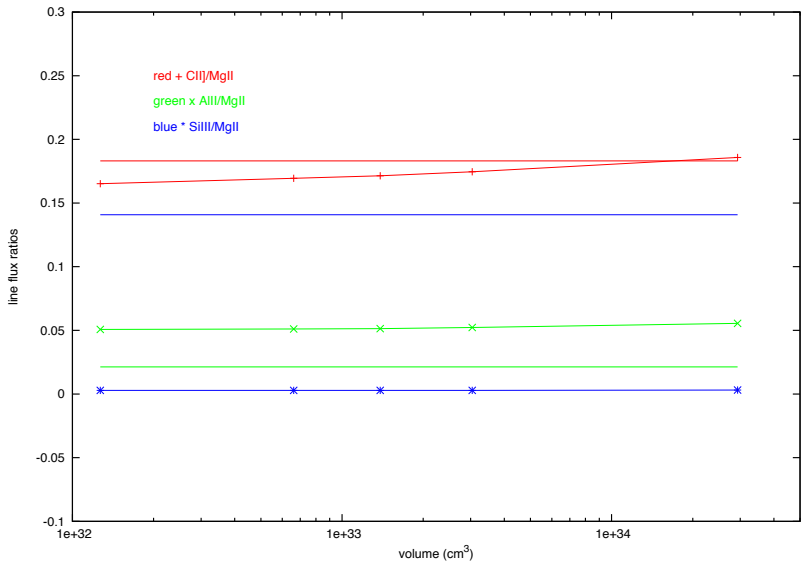

Figure 9. Line Flux Ratios of Chromospheric Model with changing volume. *Ratios include CII]/Mg II (red), Al II/MgII (green), SiIII/MgII (blue). Lines with points show Cloudy predictions, while flat lines are observed line ratios from EY Hya. Hydrogen density = 10^{10} cm^{-3} , T_{chr} =1.9x10^4 K, r_{in} =10^{10} cm were kept fixed for all models. The outer radius was the input parameter varied to change the volume.*

3.1.2.2 Adapting chromosphere component model

The chromospheric model can also be adapted to model the high-velocity emission-line blob in V Hya. Out of the optical lines listed in Table 3, only S II at 4074 Å and Ca II at 3933 Å are listed in the Cloudy output. From observations (Sahai et al. 2003), we can estimate the R_{in} and R_{out} of the blob, $10^{14.017}$ cm and $10^{14.317}$ cm, respectively. The input parameters for this model are listed in Table 6. This model did not yield line fluxes seen in observational data, and uncovered an unexpected problem resulting from including the low-temperature blackbody representing the AGB (primary) star in V Hya (section 3.2.1).

TABLE 6
MODEL AND OBSERVED LINE FLUXES FOR V HYA

	Ca II 3934 Å	**S II 4074 Å**	**T_{bb}** (K)	**T_{chr}** (K)	**Luminosity** (erg/s)	**r_{in}** (cm)	**r_{out}** (cm)	**Hydrogen Density** (cm^{-3})
epoch 7444	2.88x10^{-15}	1.76x10^{-14}	-	-	-	-	-	-
epoch 7630	5.51x10^{-15}	1.02x10^{-14}	-	-	-	-	-	-
epoch 8105	3.41x10^{-14}	4.05x10^{-14}	-	-	-	-	-	-
epoch 8134	6.45x10^{-14}	3.12x10^{-14}	-	-	-	-	-	-
Chrom model 1	6.53x10^{-13}	2.19x10^{-10}	9.5x10^3	1.2x10^4	$10^{37.32}$	$10^{14.017}$	$10^{14.317}$	10^9
Chrom. model 2	1.85x10^{-12}	4.78x10^{-10}	-	1.2x10^4	-	$10^{14.017}$	$10^{14.317}$	10^9

3.1.2.3 Fe II line Intensities

While using the code Cloudy, we encountered various issues in implementing these models. In the early stages of modeling EY Hya's chromosphere, our model spectra always produced a Fe II line at 2400 Å (Fig. 5, 6), however our literature survey (e.g. Ingleby et al. 2011) showed that Fe II does not have a line at 2400 Å. In Cloudy, the code's default is to include the lowest 16 levels of the Fe+ ion accurately (that produce IR emission), but to use a simplified scheme for the higher levels that produce optical and UV emission (Wills et al. 1985). By entering the command "atom FeII 371" into the input file, we can force Cloudy to include a complete, far more accurate model of Fe II. By adjusting the code this way, we were able to remove the false Fe II 2400 Å line from the predicted spectrum.

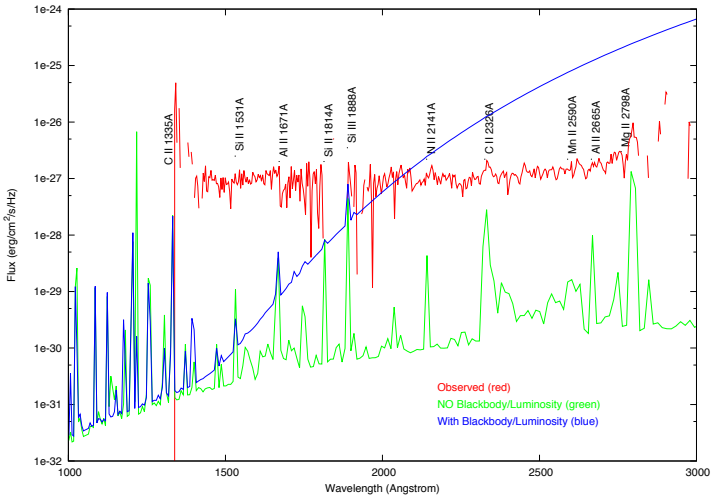

Figure 10. Chromospheric Model including a blackbody. *Modeled with a chromospheric temperature of 19,000 K, hydrogen density of 10 (log cm^{-3}), an inner radius of 10^{11} cm and an outer radius of $10^{11.04}$ cm. When a blackbody temperature of 2,900K and a luminosity of 10^{4} L_{sun} are applied, the continuum varies drastically (blue). (chromospheric model not containing a blackbody temperature or luminosity (green), has not been scaled to fit the observed spectrum (red).)*

3.2 Future Work

3.2.1 Adding a central blackbody to Chromospheric component

An unresolved issue we ran into was trying to include a central blackbody into our chromospheric models. We predicted that by including a blackbody T_{bb}=2,900K we'd reproduce emission lines typical of emission from a collisionally-ionized gas blob, with the addition of a weak continuum. But we find that this is not the case (Fig. 10). In addition to the difference in the continuous spectrum, the line fluxes listed showed significant differences between the two models for a variety of ionic lines. For example, the Mg II 2798 Å increases with the addition of the blackbody and luminosity, while the H I 1216 Å decreases. However, the CII] 2326 Å and Al II 1671 Å line fluxes are relatively unaffected.

In addition to adding a blackbody to EY Hya, we also added a central blackbody to the V Hya model introduced in Section 3.1.2.2. We know V Hya to have a luminosity of 5414 L_{sun} (De Beck et al. 2010) and an effective temperature to be ~ 2800 K (Dyck & van Belle 1996). The parameters for this model are listed in Table 6. However, our model fluxes are not close to observations (listed in Table 56. This issue currently remains unresolved. Our current explanation is that this must be due to a change in these source function for each line, since these lines are optically thick (e.g. optical depth Ca II is 67.1, from chromospheric model 2 of V Hya).

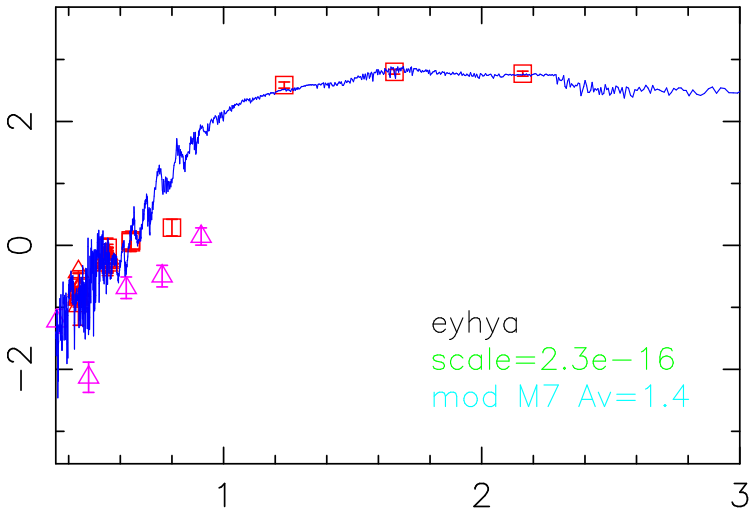

Figure 11. Model of the SED of the AGB star in EY Hya.

3.2.2

Given the issue examined in section 3.2.1, we will also need to investigate the effect of the photoionization radiation from the hot-spot on the chromospheric component.

3.2.3 Extinction of Central Object

An unresolved issue we have yet to account in our modeling is to correct for extinction (A_v) of the UV. Most of the extinction comes from the circumstellar dust, not the interstellar medium; the latter contribution is likely within the range of uncertainty to which we can determine A_v. We obtained photometric data from a variety of sources, including WISE, GALEX, SDSS and USNO for EY Hya. In order to model the SED, we normalized the model to match the 2MASS H and K photometric data (at 1.63 and 2.19 microns, respectively), and then varied A_v to get a fit for the remaining SED. Our best fit required an A_v of 1.4 (Fig. 11). When comparing the expected short-wavelength prediction of the photometric model to the observed GALEX spectrum we see that A_v does in fact affect the spectrum and therefore must be taken into account for an accurate model of EY Hya. An issue we encounter with fitting the photometric data of EY Hya, however, is that there exists a dramatic variability in the optical fluxes, which in turn makes it harder to determine an accurate estimate for A_v. In order to incorporate the effect of variability, we need to scale the optical photometry correctly to the GALEX observation epochs and also determine how the spectral type depends on the light curve phase.

4. Results

We have constructed a two-component model of EY Hya. Each component simulates starkly different physical conditions of the UV emitting region in the central object. Neither component alone is adequate for replicating the observed emission seen in EY Hya. Table 7 displays the various input parameters used to compute the accretion disk and chromospheric models for EY Hya. Therefore, our model of EY Hya includes both physical processes, the first a photoionized "hot spot" due to accretion activity around the companion and the second "chromospheric" emission from collisionally-ionized plasma. Thus, these two components (parameters seen in Table 6) create our complete two-component model of EY Hya (Fig. 12).

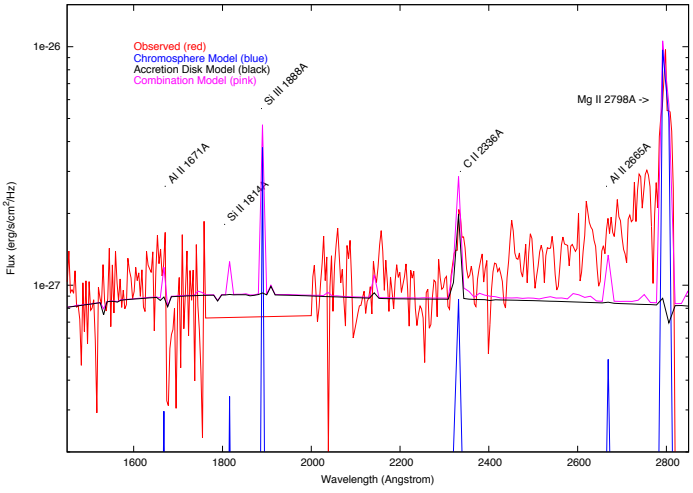

Figure 12. Chromospheric-Accretion Disk Combination Model of EY Hya. *Data between 1775 Å and 2000 Å are masked because of the very low signal/noise (S/N) ratio in this region. Observed (red), accretion activity hot spot component (black), chromospheric component (blue), and our final two-component model (pink).*

TABLE 7

LIST OF BEST FIT INPUT PARAMETERS FOR RELEVANT MODELS, INCLUDING RANGES INVESTIGATED

Object	**Type**	**T_{bb}** (K)	**T_{chr}** (K)	**Luminosity** (erg/s)	**r_{in}** (cm)	**r_{out}** (cm)	**Hydrogen Density** (cm^{-3})	**Figure**
EY Hya	Accr.	**$2.7x10^4$** $1.0x10^4$ ↓ $5.3x10^4$	-	**10^{33}** 10^{31} ↓ 10^{35}	**10^{13}** 10^{10} ↓ 10^{14}	**10^{15}** 10^{14} ↓ 10^{16}	**$10^{5.5}$** 10^3 ↓ 10^9	1
EY Hya	Chrom.	-	**$1.9x10^4$** $2.0x10^3$ ↓ $3.0x10^4$	-	**10^{11}** 10^{10} ↓ 10^{12}	**$10^{11.04}$** 10^{10} ↓ 10^{13}	**$10^{10.5}$** 10^7 ↓ 10^{13}	4
EY Hya	Chrom.	**$2.9x10^3$** $2.6x10^3$ ↓ $3.0x10^3$	**$1.9x10^4$**	**$10^{37.58}$**	**10^{11}**	**$10^{11.04}$**	**10^{10}**	10
V Hya	Chrom.	-	**$1.2x10^4$** $1.0x10^4$ ↓ $4.0x10^4$	-	**$10^{14.017}$** $10^{13.5}$ ↓ $10^{15.017}$	**$10^{14.317}$** 10^{12} ↓ $10^{15.317}$	**10^9** 10^8 ↓ 10^{13}	-
V Hya	Chrom. w/ bb	**$9.5x10^3$** $6.0x10^3$ ↓ $1.0x10^4$	**$1.2x10^4$** $1.0x10^4$ ↓ $1.5x10^4$	**$10^{37.32}$**	**$10^{14.017}$** $10^{13.5}$ ↓ $10^{15.017}$	**$10^{14.317}$** 10^{12} ↓ $10^{15.317}$	**10^9** 10^8 ↓ 10^{13}	-

***Bolded parameters are best fit**

**Smaller parameters are ranges explored

5. Conclusion

The results presented here highlight a technique to model UV emission due to a binary companion and/or accretion activity around fuvAGB stars using with the code, Cloudy. We focus our attention on the object EY Hya because it has the most extensive UV data (FUV and NUV spectra and broadband photometry). Modeling emission typical of an AGB star from EY Hya alone does not replicate the observed spectrum. We find that its UV spectrum can be explained when computing combined affects of photoionization due to accretion activity from a hot spot as well emission from a collisionally-ionized chromosphere around either EY Hya or its companion. The general lack of emission lines in the accretion disk component, and the absence of the continuum from the chromospheric component, confirms that a two-component model is needed. These results open the door for a new technique for modeling binarity of AGB stars with FUV and NUV excess shortward of 3000 Å.

Appendix

A.1 Cloudy creates multiple output files. By using the command *punch name.con* in the input, where *name* is user-specified, the output of the code produces a list of wavelength and total emission; sum of transmitted and reflected continua and lines: νF_ν [erg cm^{-2} s^{-1}]. We use this data to create the predicted spectrum, F_ν . We have to scale the predicted flux by $\left(\frac{r_{in}}{D}\right)^2$ to compute the flux at Earth. The main output of the code is identified as *name.out*, where *name* is user-specified during the creation of your input file, *name.in*. The line fluxes used for our analysis are "emergent line fluxes", (i.e., the emission observed from outside the cloud). The units of the final printout of the line fluxes in the Cloudy output file will depend on whether the luminosity case is specified (as it was for the accretion activity hot spot model) or the intensity case (as it was for the chromospheric model) . The line fluxes are in units of erg s^{-1} for the luminosity case, and erg s^{-1} cm^{-2} for the intensity case. To get the line fluxes in comparable units of erg s^{-1} cm^{-2} as well as scaled to the appropriate distance, we divide the flux in the luminosity case by $4 \pi D^2$, where D is the distance to the object, and multiply the flux in the intensity case by $\left(\frac{r_{in}}{D}\right)^2$.

A.2 For our models, we have to specify the geometry of the environment. Since the gas fully covers the center of symmetry, we must utilize the command "sphere" which then sets the covering factor, the fraction of 4π sr covered by the gas as viewed from the central source of ionization radiation, to a value big enough to allow the continuous radiation that escape the cloud in the direction towards the central object, to always interact with gas on the other side. From hazy 3, the third installation of Cloudy's manual, "In an open geometry the inward part of the line includes the effects of extinction between the line-forming region and the illuminated face. There is an additional contribution due to reflection off the gas in the outward direction. The outward part of the line includes the effects of extinction between the shielded face and the point where the line forms. In a closed geometry the emergent intensity is the emission escaping to the outer edge of the slab." In our case, the chromosphere model was calculated using closed geometry because the "sphere" command was utilized, while the accretion disk model was computed using open geometry.

A.3 When specifying the chromospheric temperature in the Cloudy input, the command "coronal equilibrium, *temperature* K" where temperature is user specified, is utilized.

Acknowledgments

We thank Gary Ferland for the use of the code Cloudy. The authors' research described here was carried out at the Jet Propulsion Laboratory, California Institute of Technology, under contract with NASA. A.C.S gratefully acknowledges the support of the Universities Space Research Association provided through NASA's Undergraduate Student Research Program. R.S.'s financial support was provided by NASA through a Long Term Space Astrophysics and GALEX GO award.

References

Balick, B., Frank, Al. 2002, ARA&A, 40, 439
De Beck, E., Decin, L., de Koter, A., Justtanont, K., Verhoelst, T., Kemper, F., and Menten, K.M. 2010, A&A, 523, 18
Deeb, J.E., and Sahai, R. 2012, Final Report, CSU STEM Teacher & Researcher Internship
Dyck, H.M. & van Belle, G.T. 1996, AJ, 112, 294
Evans, L., T. private communication, 2011
Ferland, G. J. Korista, K.T. Verner, D.A. Ferguson, J.W. Kingdon, J.B. Verner, & E.M. 1998, PASP, 110, 761
Garcia-Segura, G. 1997, ApJ, 489, L189
Ingelby, L. et al 2011, ApJ, 743, 105
Reimers, D. & Cassatella, A. 1985, ApJ, 297, 275
Sahai, R., Findeisen, K., Gil de Paz, A., & Sanchez Contreras, C. 2008a, ApJ, 689, 1274
Sahai, R. et al. 20008b, GALEX Proposal, Cycle 5, 54
Sahai, R., Morris, M., Knapp, G.R., & Young, K., 2003, Nature, 426, 261
Sahai, R., & Trauger, J. T. 1998, AJ, 116, 1357
Skinner, C.J., Dougherty, S.M., Meixner M., et al. 1997, MNRAS, 288, 295
Wills, B.J., Netzer, H., & Wills, D. 1985, ApJ, 288, 94